Journal of Nuclear Materials 396 (2010) 240–244

Contents lists available at ScienceDirect

Journal of Nuclear Materials

journal homepage: www.elsevier.com/locate/jnucmat

XRD contribution to the study of Cs-implanted cubic zirconia

A. Debelle [a,*], A. Declémy [b], L. Vincent [a], F. Garrido [a], L. Thomé [a]

[a] Univ. Paris-Sud 11 – Centre de Spectrométrie Nucléaire et de Spectrométrie de Masse (CSNSM), CNRS-IN2P3, Bât. 108, 91405 Orsay Cedex, France
[b] Laboratoire de Physique des Matériaux (PhyMat), CNRS-Université de Poitiers, BP 30179, F-86962 Chasseneuil-Futuroscope Cedex, France

ARTICLE INFO

Article history:
Received 8 July 2009
Accepted 19 November 2009

ABSTRACT

The radiation-induced damage in Cs-implanted cubic zirconia at room temperature has been investigated as a function of the fluence (from a few 10^{13} to a few 10^{16} cm^{-2}) by means of XRD measurements. These experiments allowed determining the maximum strain and stress experienced by the damaged layers as well as the strain depth profiles. The radiation-induced elastic strain, localized along the direction normal to the implanted sample surface, is positive. It induces an in-plane compressive stress which reaches −1.6 GPa before relaxation. This strain essentially comes from ballistic collisions generating interstitial-type defects, but a contribution due to Cs incorporation into the matrix should also be taken into account. XRD data have been confronted to results previously obtained by RBS/C and TEM experiments. A strong correlation between the evolution of the normal strain and of the disorder level measured by RBS/C is clearly established. In particular, the relaxation of the stored elastic strain takes place concomitantly with the microstructural evolution evidenced by the RBS/C damage build-up and imaged by TEM. Besides, the width of the strain depth profiles indicates that the strained layer is broader than the damaged thickness revealed by RBS/C and TEM analyses.

1. Introduction

One of the major challenges to build a sustainable future for nuclear energy production is the significant reduction of the nuclear waste amount, especially the highly radioactive minor actinides. For this purpose, it is planned to incinerate the actinides directly in nuclear reactors. One key to perform this operation is to use an inert matrix fuel (IMF) as transmutation matrix in which actinide oxides form stable solid solutions. Refractory oxide ceramics are the best suited materials for this application. Among the possible candidates, yttria-stabilized cubic zirconia (YSZ) is considered as one of the most promising IMF since it satisfies the crucial criterion of high radiation resistance. Indeed, it has been demonstrated that this matrix does not undergo any phase transformation or amorphization upon low or medium-energy inert gas implantation or irradiation, even at high damage level [1–3]. In addition to the high radiation tolerance, another essential property that must possess IMF is the ability to confine radiotoxic fission products, and especially caesium which has revealed to be one of the most deleterious elements for the crystalline matrix integrity. Actually, amorphization of YSZ was only observed after Cs implantation and tentatively attributed to the inability of the host matrix to accommodate the large crystalline lattice distortions induced by the presence of implanted huge Cs ions [4]. It was also shown [5–7] that the diffusion and release of Cs ions implanted into YSZ are strongly dependent on many parameters such as the Cs concentration in the doped region, the implantation or annealing temperature, the presence of other foreign atoms (e.g. iodine), the damage level of the host matrix. These results clearly emphasize the importance to study the behaviour of Cs-implanted into YSZ and the associated structural damage, in order to definitely assess the qualification of this material as IMF. Our group thoroughly aims to investigate this issue [3,8,9]. Very recently, we presented an extensive study concerning the microstructural evolution, examined by means of Rutherford Backscattering Spectrometry and Channelling (RBS/C) and Transmission Electron Microscopy (TEM), of Cs-implanted YSZ as a function of fluence and temperature [10]. Hereafter are briefly reported selected results obtained at room temperature (RT) which constitute the starting point of the present work.

At RT, the damage build-up with increasing implantation fluence was observed to evolve by discrete microstructural transformations. Actually, a multi-step process, which is commonly observed during low or medium-energy ion implantation [1,11,12], was established, involving three successive but dramatically different microstructural transformations. At high fluence ($\sim 5 \times 10^{16}$ cm^{-2}), amorphization of the damaged layer occurs, presumably due to the high Cs ion concentration incorporated into the zirconia matrix. This final stage is not treated in the present study. At the very beginning of the damage build-up, the virgin crystal transforms into a defective crystal due to ion bombardment. Small

* Corresponding author. Tel.: +33 1 69 15 35 95; fax: +33 1 69 15 52 68.
E-mail address: aurelien.debelle@csnsm.in2p3.fr (A. Debelle).

0022-3115/$ - see front matter © 2009 Elsevier B.V. All rights reserved.
doi:10.1016/j.jnucmat.2009.11.016

radiation defects are created and induce the formation of tiny distorted nanometer-sized domains (see [10]). Then, at intermediate fluences, *i.e.* at a $\sim 8 \times 10^{14}$ cm^{-2} transition fluence, Φ_{tr} (which represents $\sim$3 displacements per atom (dpa)), this damage accumulation leads to a microstructural transformation. Actually, relaxation of the structure occurs by the formation of new defects, namely 'misfit' dislocations, at the interface between the distorted domains and the undamaged surrounding matrix. At a few 10^{16} cm^{-2}, the domain and dislocation density saturates while the damaged layer broadens. This microstructural modification was tentatively attributed to the reduction of the elastic energy stored in the damaged layer. The present paper aims at proving this assumption.

In this study, the strain/stress state of Cs-implanted YSZ crystals has been investigated by means of X-ray Diffraction (XRD) measurements. The strain depth profiles and the maximum stress experienced by the damaged layers have been determined. The methodology used is described in details elsewhere [13]. The overall XRD data have been discussed in the light of the results previously obtained by complementary techniques, namely RBS/C and TEM [3,8,10].

2. Experimental

2.1. Ion implantation and ion beam characterization

The specimens used are ⟨1 0 0⟩-oriented cubic yttria-stabilized zirconia single crystals containing 9.5 mol % Y_2O_3, and synthesized by Crystal-GmbH. YSZ crystals have the fluorite structure ($Fm\bar{3}m$) with $a_0 = 0.5145$ nm (as determined from XRD measurements) and $\rho = 5.9$ g cm^{-3} (this value is issued from the refinement of a X-ray reflectivity curve). Implantations and ion beam characterizations have been performed with the JANNuS facility of the CSNSM-Orsay. Implantations were performed at RT with 300-keV Cs ions fluences ranging from a few 10^{13} to a few 10^{16} cm^{-2}. An incident beam angle of 7° was used during implantation to avoid any channelling phenomenon. Monte Carlo simulations using the SRIM code [14] were implemented in order to determine the corresponding nuclear energy loss $(dE/dx)_{nucl}$ profile. In addition, the experimental Cs depth distribution in the 3×10^{14} cm^{-2} Cs-implanted sample was determined by RBS and the damage profile in the Zr sublattice was extracted from RBS/C measurements.

2.2. XRD

XRD measurements were performed in the Bragg reflection geometry (horizontal scattering plane) on a four-circle Seifert XRD-3000 goniometer (at the PhyMat, Poitiers) using a line focus Cu X-ray source. A Ge (2 2 0) double-crystal monochromator and a 0.1 mm primary slit provided a parallel and monochromatic ($\lambda = 0.15406$ nm) incident X-ray beam and a 0.07 mm detector slit allowed a 2θ angular resolution of 0.01°. Symmetric θ–2θ scans were recorded in the vicinity of the (4 0 0) Bragg reflection ($2\theta_{(400)} \sim 73.575°$) of the (fluorite-type) zirconia, which ensured a relatively high resolution due to the high scattering angle.

The formalism used in this work is described in [13]; it is here restricted to the study of planes parallel to the surface, *i.e.* {1 0 0} planes. It has been demonstrated that the radiation-induced strain in low-energy ion-implanted materials is localized along the direction normal to the implanted sample surface. To determine this normal strain, only symmetric θ–2θ scans around (h 0 0) Bragg planes are required. Indeed, in this case, the reciprocal lattice vectors corresponding to the {1 0 0} planes and the deviation vectors from these reciprocal lattice vectors are collinear and have a normal component only. In this study, these vectors will be labelled as H_{400} and q_N, respectively. Fig. 1 represents the result of such scans for the virgin and as-implanted samples. It must be mentioned that on the curves corresponding to the implanted zirconia samples appear fringe patterns. Their fitting allows determining the normal strain depth profile as shown below. In this study, θ–2θ curves were simulated by using the GID_sl web-based program [15].

3. Results

Fig. 1 displays the θ–2θ experimental scans recorded in the vicinity of the (4 0 0) Bragg reflection for virgin and implanted zirconia specimens; note that the (logarithmic) intensity distributions are also plotted as a function of the normalized deviations from the reciprocal lattice vector. The quantity $(-q_N/H_{(400)})$ is equal, provided that deviations are weak, to ε_N, the elastic strain in the direction normal to the surface of the samples. The intense narrow peak on the high-angle side of the scans ($2\theta - 73.6°$) and corresponding to the unperturbed part of the samples is taken as an internal strain gauge to quantify this normal strain. It must be pointed out that the position of the last peak located at the lowest 2θ angle of the XRD curves provides a good approximated value of the maximum normal strain magnitude (ε_N^{max}) exhibited by the irradiated layer [13].

The XRD curves displayed in Fig. 1 are very similar from 3.75×10^{13} cm^{-2} up to 7.5×10^{14} cm^{-2} fluence, *i.e.* in the fluence range corresponding to the first step of the damage build-up. They show three important features: (i) the XRD signal arising from the damaged part of the samples is located at lower angles relatively to the peak corresponding to the undamaged region. This indicates that the perturbed layer is characterized by a larger lattice parameter, thus it exhibits a positive (tensile) normal strain; (ii) the position of the last peak located at the lowest 2θ angle moves toward lower angles when the fluence increases. This shift signs a rise of the maximum normal strain magnitude (ε_N^{max}); (iii) the fringe spacing shrinks with increasing fluence, pointing out an increase of the width of the strain profile. At $\sim 5 \times 10^{15}$ cm^{-2}, *i.e.* above the second

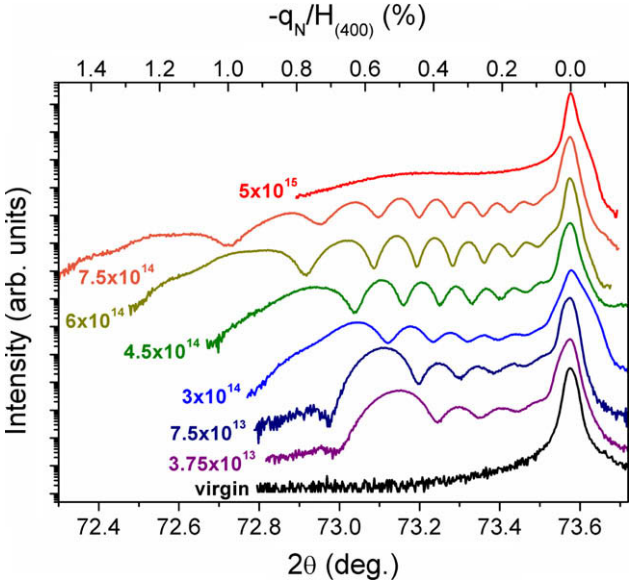

Fig. 1. θ–2θ scans recorded in the vicinity of the (4 0 0) Bragg reflection of virgin and 300 keV Cs-implanted YSZ single crystals at different fluences. For visualization purposes, each curve is multiplied by an arbitrary factor. Note that the intensity plotted in logarithmic scale is also displayed as a function of the normalized deviation from the reciprocal lattice vector $(-q_N/H_{(400)})$, which is equal to the elastic strain in the direction normal to the surface sample.

structural transition, the fringe pattern disappears. The remaining very wide peak corresponding to the damaged part of the sample must be ascribed to diffuse scattering arising from a highly defective crystalline lattice. Moreover, this scattering signal dramatically moves closer to the unperturbed zirconia diffraction peak, revealing a large strain relief. This has already been observed under different irradiation conditions in YSZ [16] and also e.g. in pyrochlores [17].

Fig. 2a presents the evolution with the implantation fluence (and with the damage dose expressed in dpa) of ε_N^{max} directly obtained, in the range where fringe patterns are observed, from the position of the last peak on the low-angle side on the θ–2θ curves displayed in Fig. 1. It must be mentioned that this value is the sum of two contributions, as described in [13]: (i) a "free" strain due to a volume lattice change induced by the radiation defects, and (ii) a strain arising from the thick undamaged layer reaction. It is worth noting that the total maximal normal strain ε_N^{max} is already ~0.5% at the lowest investigated fluence (3.75×10^{13} cm^{-2} to 0.16 dpa) and reaches a value larger than 1.2% just before Φ_{tr}. Fig. 2b displays the corresponding biaxial in-plane stress $\sigma_{\parallel}^{max}$ experienced by the damaged layer, calculated as described in [13]. It must be noted that this compressive stress amounts to a huge level of approximately −3.6 GPa just before the formation of the relaxation misfit dislocations. Moreover, at Φ_{tr}, the corresponding (hydrostatic) stress, which arises only from the defect-induced lattice volume change, reaches ~4.8 GPa. This positive value is indicative of an expansion of the zirconia lattice due to the creation of radiation-induced defects, and its amplitude directly reflects the large defect concentration.

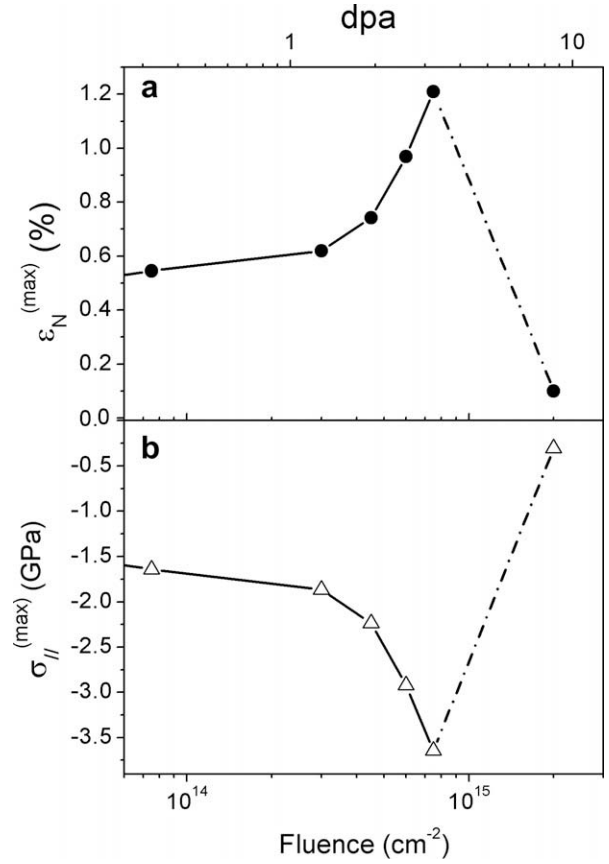

Fig. 2. Evolution as a function of the Cs implantation fluence and of the damage dose (expressed in dpa) of (a) the maximum elastic strain XRD (ε_N^{max}), and (b) the maximum in-plane biaxial stress ($\sigma_{\parallel}^{max}$) exhibited by the YSZ implanted layers. The size of the symbols corresponds to the error bar. Solid lines are just guides to the eyes.

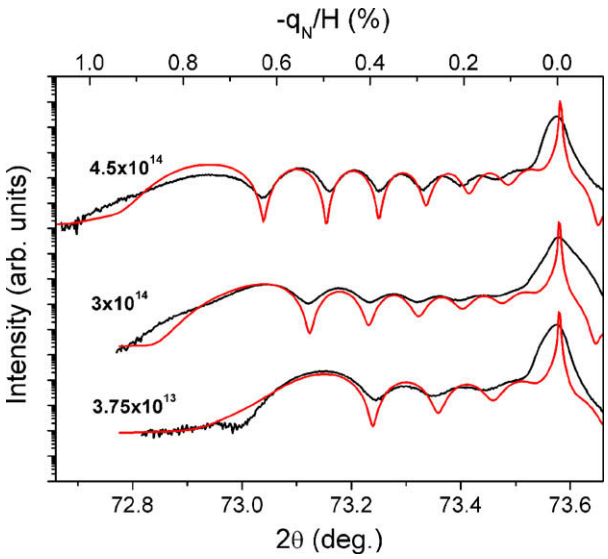

Fig. 3. Experimental θ–2θ scans (black lines) on the (4 0 0) Bragg planes of Cs-implanted YSZ at different fluences and corresponding simulated curves (red lines) obtained from the strain profiles shown in Fig. 4. (For interpretation of the references to colour in this figure legend, the reader is referred to the web version of this article.)

Fig. 3 shows the best fits obtained from the refinement, with the GID_sl program, of experimental data corresponding to three different implantation fluences selected before the (main) structural transformation at Φ_{tr} (*i.e.* before the fringe pattern disappearance). It can be noted that the fringe periods are well reproduced by the simulated curves. Therefore, the proposed simulated strain depth profiles (see Fig. 4) reasonably reflect the shape, and especially the width, of the strain profiles present in the implanted layers. The choice of the depth scale is discussed hereafter. It is worth mentioning that, in the present case, no static Debye–Waller factor [18] has been introduced, which explains, considering also that the experimental resolution has not been taken into account, that the proposed simulated curves do not perfectly reproduce experimental intensities. As shown in Fig. 4, whatever the implantation fluence, all implanted crystals exhibit a strain depth profile presenting the same overall shape which roughly describes a broad Gaussian-like curve. However, the maximum strain level increases with the fluence, as expected from data of Fig. 1, as well as the width of the profiles, in agreement with RBS/C results and TEM observations [10].

4. Discussion

Fig. 5 presents the variation with both the implantation fluence and the damage dose (expressed in dpa) of the disorder level determined by RBS/C, and the variation of the maximal total normal strain deduced from XRD measurements. It is worth noticing that, at the lowest fluences, RBS/C is almost insensitive to radiation damage, contrary to XRD which already reveals a relatively large elastic strain level. Notwithstanding this difference, the two evolutions appear strongly linked, and the elastic strain reveals to be, as the f_D parameter, a quantitative measure of the disorder level. The two kinetics can be described as follows: (i) at low fluences, ε_N^{max} first increases very slowly and, from ~3×10^{14} cm^{-2}, its augmentation rate rapidly increases; meanwhile, f_D exhibits a monotonous and smooth increase; (ii) at a same transition fluence ($\Phi_{tr} \sim 8 \times 10^{14}$ cm^{-2}), both parameters display a sudden and dramatic evolution: f_D strongly increases while the strain is relaxed. It has been shown by TEM that the progressive rise of f_D during

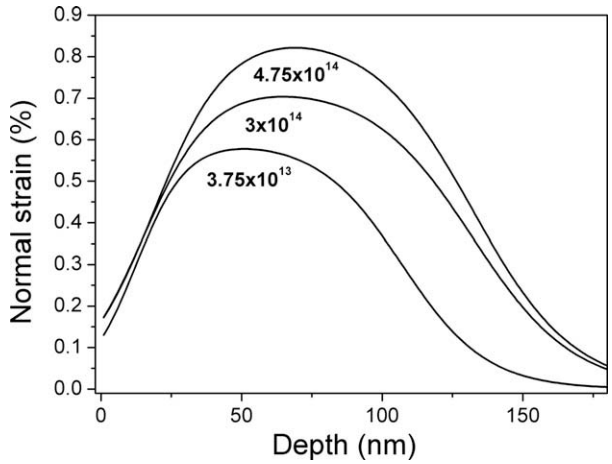

Fig. 4. Simulated strain depth profiles in Cs-implanted YSZ at different selected fluences.

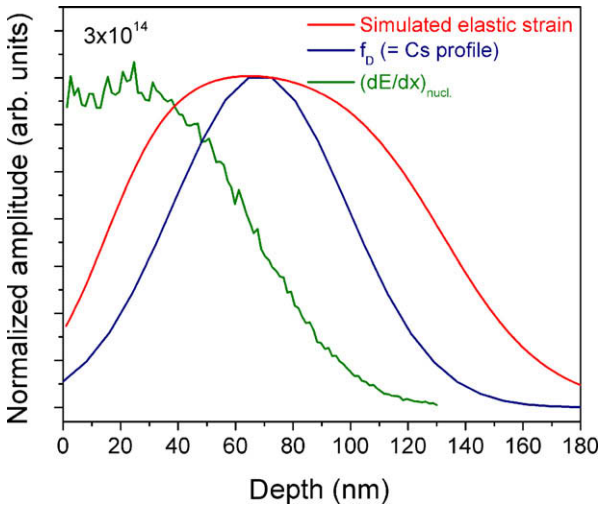

Fig. 6. Comparison of the depth profile of (i) the nuclear energy loss, (ii) the Cs atoms, (iii) the damage and (iv) the elastic strain. All curves are normalized to the maximum elastic strain level.

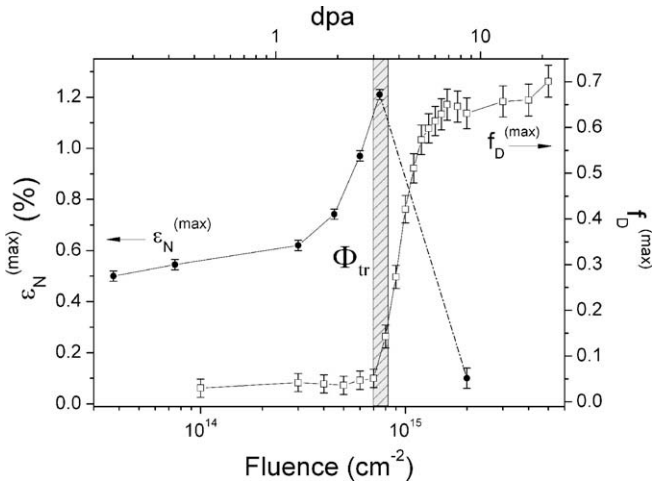

Fig. 5. Comparison of the variation as a function of the Cs implantation fluence and of the damage dose (expressed in dpa) of the maximum elastic strain (ε_N^{max}) and of the disorder level (f_D). Symbols are experimental data and lines are guide to the eyes.

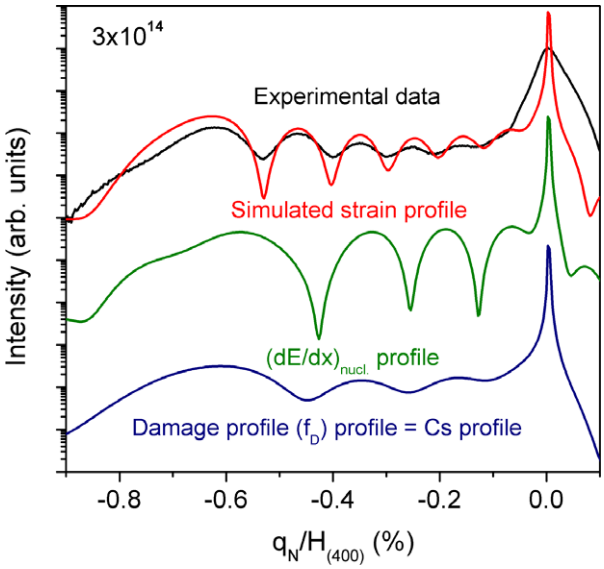

Fig. 7. θ–2θ simulated curves of the experimental data (black line) corresponding to the 3×10^{14} cm^{-2} implanted crystal taking as possible strain depth profiles the nuclear energy loss profile (blue line), the experimental damage depth distribution (green line), and the proposed simulated strain profile (red line) (see Fig. 6). (For interpretation of the references to colour in this figure legend, the reader is referred to the web version of this article.)

the first damage step arises from the formation of distorted nanometer-sized domains with a density increasing with implantation fluence. Thus, the radiation-induced defects at the origin of the formation of these domains induce first lattice distortions which generate elastic strains (and stresses) whose level increases with the fluence. Then, at the transition fluence Φ_{tr}, a huge strain/stress relief along with a large increase of the disorder level (as seen by RBS/C) occur, both phenomena being due to the formation of (relaxation) misfit dislocations. Consequently, the assumption that the structural transformation occurs to relax the radiation-induced elastic strain (or stress) is here clearly confirmed. In other words, it is demonstrated in this work that the elastic strain is a key parameter that triggers microstructural evolutions of YSZ under irradiation.

Fig. 6 displays the depth distribution at 3×10^{14} cm^{-2} of the damage (RBS/C), the Cs atoms (RBS), and the nuclear energy loss (SRIM calculations). The profiles are normalized to the maximum elastic strain. Usually, it is found that the strain depth profile overlaps on one of the three above mentioned profiles [19–21]. Hence, as a starting point, the experimental damage profile (f_D), which is here found identical to the Cs distribution, and the theoretical nuclear energy loss profile $(dE/dx)_{nucl}$, were taken as possible strain profiles. The corresponding simulated XRD curves are plotted in Fig. 7. The poor agreement between experimental data and calculations demonstrates that none of these two profiles is appropriate. In particular, the fringe number is not reproduced. Actually, several fringes are lacking, which indicates that the width of these two profiles is not large enough. However, their shape and depth location are useful information for the determination of that of the simulated strain depth profile (it must be mentioned that the absolute depth location of a strain profile, as well as its asymmetry with respect to its maximum, are undetermined from such XRD measurements [22]). Actually, the depth scale of the strain distribution displayed in Fig. 6 has been, for comparison, arbitrarily chosen considering that of the experimental damage profile. This proposed strain profile gives the best-fit XRD curve plotted in Fig. 7. Its width is much larger than that of the two other tested profiles taken

separately, but it is roughly consistent with the thickness corresponding to the sum of both contributions. This feature is found for all the investigated fluences.

The measured positive strain is induced by defects which generate a lattice swelling. Different types of such defects can be formed with the present irradiation conditions. Damage can arise from ballistic collisions creating self-interstitial atoms (SIA) which may cluster or remain as isolated point-like defects, or from the incorporation of impurities, *i.e.* Cs atoms in substitutional and/or in interstitial positions. The damage measured by RBS/C cannot be attributed to the presence of Cs atoms, since (i) the Cs concentration is very small (~0.13% at the maximum of the implantation profile at Φ_{tr}), and (ii) a weak increase of the Cs content cannot explain the huge rise of f_D at the end of step 1. On the contrary, the increase of the backscattering yield measured in the first step can very likely be due to the presence of the distorted domains observed by TEM which are induced by the creation of SIAs generated by ballistic collisions. The re-arrangement of these defects into dislocations can then explain the sudden and dramatic f_D evolution above Φ_{tr}. The situation is not that straightforward concerning elastic strain measured by XRD. If the role of ballistic defects to the strain build-up appears indubitable, the contribution of the (Cs) foreign atoms cannot be ruled out. Actually, in the case of small defects, the strain is directly related to the defect concentration, c_j, through the equation [23]:

$$\varepsilon^{(\mathrm{def})} = \sum_j c_j \frac{V_j^{\mathrm{rel}}}{\Omega} \quad (1)$$

where V_j^{rel} is the relaxation volume of the defects expressed in atomic volume unit, Ω. Note that $\varepsilon^{(\mathrm{def})}$ is not the measured normal strain, but the free strain only due to the defect-induced lattice volume change (*i.e.* without the component due to the substrate reaction, see [13] for more details). Assuming an average relaxation volume of 1 Ω for each incorporated Cs atom, the strain induced by the presence of Cs atoms would be of the order of 0.13% at the transition fluence and at the maximum of the strain depth distribution, as compared to a maximum free strain of ~0.8%. Hence, Cs atoms would contribute to ~1/4 of the total measured normal strain. This contribution cannot be *a priori* disregarded, and on the contrary, should rather be taken into account. Besides, this contribution could explain the increase in the augmentation rate of the strain during the first damage step which is not observed for the disorder level measured by RBS/C. Finally, the strain profiles would arise from the superposition of two strain fields: the first one due to a ballistic contribution generating host atoms displaced from their initial crystallographic position (self-interstitial atoms), and the second one due to the incorporation of Cs atoms into the lattice. Nevertheless, more work is required to get better insight on these two contributions to the observed normal strain profile.

5. Conclusion

The radiation damage produced in cubic yttria-stabilized zirconia implanted with Cs ions at RT has been studied by XRD, and the contribution of this technique to the study of ion-implanted materials has been demonstrated. It is found that the elastic strain constitutes a direct quantitative measure of the radiation-induced disorder level. The damage build-up as determined by monitoring the variation of the strain exhibits two steps. An increase of the strain experienced by the damaged layer, due to the formation of radiation-induced defects, is observed in the first step. This out-of-plane strain is positive and induces an in-plane compressive stress which amounts up to −3.6 GPa at the transition fluence. At this fluence, a dramatic strain relaxation occurs. This second step arises from the formation of misfit dislocations and takes place to reduce the elastic strain stored in the damaged layer. Furthermore, ion implantation generates a strain depth profile with a width and a maximum level that increase with increasing fluence. This behaviour is in agreement with TEM and RBS/C results.

The experiments presented in this study provide a strong indication that the minimization of the system energy, and particularly the elastic energy, is a driving force for microstructural transformations of YSZ under irradiation to occur. This result should thus be taken into account in further studies and for other materials in the field of ion beam modifications of materials.

Acknowledgements

One of the authors (A. Debelle) would like to warmly thank Sergey Stepanov for rapidly and kindly inserting in the GID_sl program the data relative to the zirconia matrix for the simulation of the XRD curves.

References

[1] K.E. Sickafus, Hj. Matzke, Th. Hartmann, K. Yasuda, J.A. Valdez, P. Chodak III, M. Nastasi, R.A. Verall, J. Nucl. Mater. 274 (1999) 66.
[2] W.L. Gong, W. Lutze, R.C. Ewing, J. Nucl. Mater. 277 (2000) 239.
[3] L. Thome, J. Fradin, J. Jagielski, A. Gentils, S.E. Enescu, F. Garrido, Eur. Phys. J.: Appl. Phys. 24 (2003) 37.
[4] L.M. Wang, S.X. Wang, R.C. Ewing, Philos. Mag. Lett. 80 (2000) 341.
[5] L. Thomé, A. Gentils, F. Garrido, J. Jagielski, Prog. Nucl. Energy 38 (2001) 277.
[6] M.A. Pouchon, M. Döbeli, C. Degueldre, M. Burghartz, J. Nucl. Mater. 274 (1999) 61.
[7] M.A. Pouchon, C. Degueldre, M. Döbeli, Prog. Nucl. Energy 38 (2001) 275.
[8] A. Gentils, M.-O. Ruault, L. Thomé, J. Nucl. Mater. 381 (2008) 297.
[9] A. Gentils, S.E. Enescu, L. Thome, H. Khodja, G. Blaise, T. Thomé, J. Appl. Phys. 97 (2005) 113509.
[10] L. Vincent, L. Thome, F. Garrido, O. Kaitasov, F. Houdelier, J. Appl. Phys. 104 (2008) 114904–114908.
[11] J. Jagielski, L. Thomé, Vacuum 81 (2007) 1352.
[12] F. Garrido, L. Vincent, L. Nowicki, G. Sattonnay, L. Thomé, Nucl. Instrum. Methods B 266 (2008) 2842.
[13] A. Debelle, A. Declémy, Nucl. Instrum. Methods B, in press.
[14] J.F. Ziegler, J.P. Biersack, U. Littmark, The Stopping and Range of Ions in Solids, Pergamon, New York, 1985. <http://www.srim.org>.
[15] S. Stepanov, R. Forrest, J. Appl. Crystallogr. 41 (2008) 958. <http://sergey.gmca.aps.anl.gov/>.
[16] S. Moll, L. Thomé, G. Sattonnay, A. Debelle, L. Vincent, F. Garrido, J. Jagielski, J. Appl. Phys. 106 (2009) 073509.
[17] G. Sattonnay, S. Moll, M. Herbst-Ghysel, C. Legros, J.-M. Costantini, L. Thomé, Nucl. Instrum. Methods B 266 (2008) 3052.
[18] P.H. Dederichs, J. Phys. F: Metal Phys. 3 (1973) 471.
[19] G. Lulli, M. Bianconi, A. Parisini, S. Sama, M. Servidori, J. Appl. Phys. 88 (2000) 3993.
[20] T. Emoto, K. Akimoto, K. Ito, J. Ghatak, P.V. Satyam, e-J. Surf. Sci. Nanotechnol. 4 (2006) 25.
[21] S. Leclerc, M.F. Beaufort, A. Declémy, J.F. Barbot, Appl. Phys. Lett. 93 (2008) 122101.
[22] N. Sousbie, L. Capello, J. Eymery, Ch. Lagahe, F. Rieutord, J. Appl. Phys. 99 (2006) 103509.
[23] P. Ehrhart, K.H. Robrock, H.R. Shober, in: R.A. Johnson, A.N. Orlov (Eds.), Physics of Radiation Effects in Crystals, Elsevier, Amsterdam, 1986.